Penttinen, Jenna; Nisula, Mikko; Karppinen, Maarit

Atomic/Molecular Layer Deposition of s-Block Metal Carboxylate Coordination Network Thin Films

Published in:
Chemistry: A European Journal

DOI:
10.1002/chem.201703704

Published: 01/12/2017

Document Version
Peer-reviewed accepted author manuscript, also known as Final accepted manuscript or Post-print

Please cite the original version:
Penttinen, J., Nisula, M., & Karppinen, M. (2017). Atomic/Molecular Layer Deposition of s-Block Metal Carboxylate Coordination Network Thin Films. *Chemistry: A European Journal*, *23*(72), 18225-18231. https://doi.org/10.1002/chem.201703704

Atomic/Molecular Layer Deposition of s-block Metal Carboxylate Coordination Network Thin Films

Jenna Penttinen, Mikko Nisula, and Maarit Karppinen*[a]

Abstract: We present novel atomic/molecular layer deposition (ALD/MLD) processes for the fabrication of crystalline inorganic-organic coordination network thin films with different s-block elements; terephthalic acid is employed as the organic precursor. Such thin films could enable e.g. next-generation battery, sensor and gas-storage technologies. The deposition processes fulfill the basic principles of ALD/MLD-type growth including the sequential self-saturated gas-surface reactions and atomic/molecular-level control for the film thickness, and yield crystalline thin films in a wide deposition temperature range. Structural characterization of the films is performed by GIXRD and FTIR; the data do not unambiguously prove but also do not rule out the crystal structures previously reported for the corresponding bulk samples. We moreover demonstrate the growth of crystalline thin films of a new terephthalate material with La as the metal component. Upon humidity treatments the Li, Na, K, Ba, and La terephthalate films remain unaffected while the Mg, Ca, and Sr terephthalate films reversibly absorb water molecules forming well-defined crystalline water-derivative phases.

Introduction

A coordination network structure consists of regularly arranged metal cations linked together with organic molecules such as different aromatic polycarboxylates; a common example of the carboxylates used is terephthalic acid.[1,2] The porous/open structures often seen for the coordination network materials allow them to be used for example for gas storage, and as sensors, smart membranes or electrochemical electrode materials;[3,4] they may also serve as a host matrix for non-native functionality by accommodating various guest species.

Coordination network structures based on alkali and alkaline earth metals have been little investigated even though they could bring new attractive aspects for the next-generation sustainable applications.[5–8] Firstly, alkali and alkaline earth metals are non-toxic and environmentally benign, and on top of that, many of them (Na, K, Mg and Ca) are earth-abundant and appreciably cheap. Also, interesting new chemistry features could be expected as the alkali and alkaline earth elements are more electropositive than the transition metals, forming thus stronger ionic bonds to the carboxylate oxygen atoms.[2] Owing to the ionic bonds, the s-block metal based structures are more prone to absorb guest water molecules than the transition metal based structures.[9,10] In these hydrolyzed coordination networks, the water molecules can be coordinated either directly to the metal cation or to the organic linkers via hydrogen bonds.[10]

Together with terephthalic acid (1,4-benzenedicarboxylic acid; TPA) both alkali (Li, Na and K) and alkaline earth (Mg, Ca, Sr and Ba) metals are known to form layered coordination network structures with alternating metal oxide and anionic terephthalate (TP) layers where the metal cation is in a bridging position, see Figure 1.[8,11–14] The smallest alkali metal lithium favours tetrahedral coordination, whereas sodium, potassium, calcium and strontium coordinate to six and barium to eight oxygen atoms from the TP ligands. The structures differ accordingly in the way the TP oxygen atoms are bonded to the metal cations, as each oxygen may be bonded to either one or two metal cation.

For the alkali metal terephthalates no water-containing derivatives have been reported; in contrast, calcium and strontium terephthalates are known to readily accommodate guest water molecules to form trihydrated (Ca/Sr)$C_8H_4O_4(H_2O)_3$ structures where the water molecules are coordinated to the metal atoms to increase their coordination numbers.[8,13] Interestingly, for magnesium, even though the dry MgTP structure has not been realized the water-containing $MgC_8H_4O_4(H_2O)_2$ structure is known in which magnesium is coordinated to four TP ligands and two water molecules (Figure 1).[11] In bulk form the $MgC_8H_4O_4(H_2O)_2$ structure can be precipitated from a solution of ammonium terephthalate in aqueous ammonia by an appropriate magnesium salt solution.[15]

[a] J. Penttinen, M. Nisula, Prof. M. Karppinen
Department of Chemistry and Materials Science
Aalto University
FI-00076, Aalto, Finland
E-mail: maarit.karppinen@aalto.fi

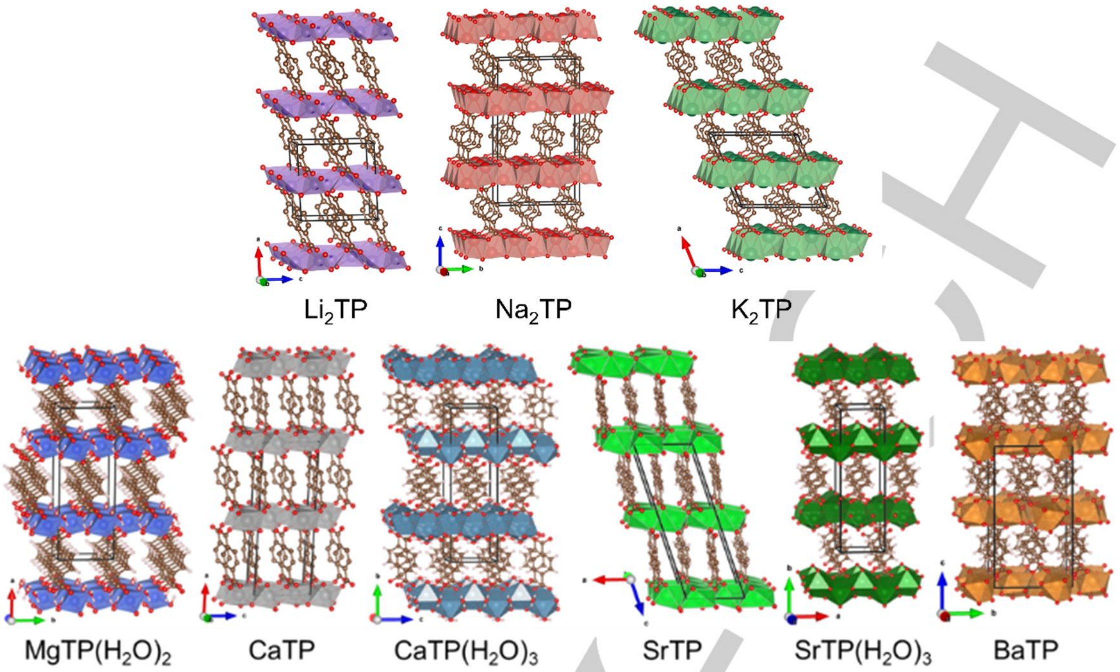

Li_2TP Na_2TP K_2TP

$MgTP(H_2O)_2$ CaTP $CaTP(H_2O)_3$ SrTP $SrTP(H_2O)_3$ BaTP

Figure 1. Coordination network structures (both anhydrous and hydrated) with alternating metal oxide and terephthalate anion layers identified for bulk alkali and alkaline earth terephthalate samples;[11–14,16,17] structures drawn using VESTA software.

From the application point of view, new fabrication methods and in particular techniques allowing the material to be deposited in thin-film form are required to take the full advantage of the unique properties of coordination network structures and extend their use to applications such as sensing and microelectronics.[18] However, the present solution-based deposition methods employed for the fabrication of coordination framework thin films may not be easily scalable for industrial production.[19] Another potential difficulty arises from the fact that e.g. in the sensor applications it is beneficial for the thin-film material to contain open metal sites to enhance the absorption of the guest molecules,[20] and the inherent drawback of the solution-based deposition techniques is the nearly unavoidable inclusion of the solvent molecules on these sites.[4]

The “solvent-free” gas-phase thin-film deposition techniques would obviously allow us to circumvent the solvent-inclusion problem. In particular, atomic layer deposition (ALD) is a well-known thin-film technology commercially used to fabricate high-quality thin films of inorganic materials even on various complex or otherwise demanding surface architectures. It is based on self-limiting gas-surface reactions of alternating gaseous precursors – a fact that enables the thin film uniformity and precise thickness control. Most importantly, by combining the ALD technique for inorganic materials with the currently strongly emerging molecular layer deposition (MLD) technique for organics, it is possible to deposit inorganic-organic materials in a well-controlled layer-by-layer manner.[21–26] Like ALD, the MLD technique is based on sequential and self-limiting gas-surface reactions.

Hybrid inorganic-organic thin films of aromatic carboxylic acid precursors have indeed been deposited by ALD/MLD, but the majority of the films have been amorphous.[21,22] Very recently, we succeeded in growing the first in-situ crystalline ALD/MLD thin films;[27–31] in these crystalline hybrid thin films the metal constituents were copper, calcium, lithium and sodium, and in the first three cases the organic precursor was terephthalic acid. Hence, with the exception of the Cu-terephthalate films,[27] all the other ALD/MLD processes yielding crystalline films have been based on s-block metals; noteworthy, these metals usually form ionic compounds with organic linkers.[10] We tentatively believe that the non-directionality of the ionic bond might be advantageous for the crystallization of the films during the film growth by providing the organic molecules with more freedom for the proper orientation, while the directional covalent bonds of transition metals may force the molecules to an unsuitable angle for the formation of the targeted crystal structure.

Having the Li_2TP and CaTP ALD/MLD processes developed, an obvious challenge was to extend the approach to the entire family of coordination network structures based on s-block metals. In this work, we report new ALD/MLD processes for Na, K, Mg, Sr, and Ba terephthalates that indeed yield crystalline thin films. Moreover, we report our preliminary results for a similar ALD/MLD process for trivalent lanthanum. Most interestingly, these films are found crystalline as well even though lanthanum terephthalate is not known in bulk form. Finally, we investigate our entire new family of crystalline metal terephthalate thin films for their water-absorption characteristics.

Results and Discussion

For all the metal constituents investigated our ALD/MLD processes based on metal-thd and TPA precursors yielded homogeneous thin films with appreciably high growth rates. The processes were first optimized for the precursor pulse lengths; in these experiments the deposition temperature was fixed to 220 °C and the number ALD/MLD cycles to 400, and the growth-per-cycle (GPC) was then calculated from the resultant film thickness determined from the XRR data; an example of a typical XRR curve for our metal terephthalate thin-film samples is shown in the inset of Figure 2 (c). In Figures 2 (a) and (b) we plot the GPC values as a function of the metal precursor pulse length varied in the range of 1 to 10 s. It can be seen that for all the processes a 2–5-s long metal precursor pulse is long enough to reach the complete saturation; for the further experiments we fixed both the metal precursor pulse and the subsequent purge lengths to 4–5 s. Then we optimized the TPA pulse length; this was done using the Na(thd) + TPA process as a representative case. From Figure 2 (c) it is seen that the saturation is reached with a 10-s long TPA pulse. This value was thus selected for the TPA pulse length (with a subsequent 20-30-s purge) for all our further experiments. It should be mentioned that very similar pulse length values are typically used for organic precursors in ALD/MLD processes.[21]

Next we investigated the feasible deposition temperature ranges for the processes; in Figures 2 (d) and (e) we plot the GPC values for all our ALD/MLD processes at different deposition temperatures; the temperature range investigated was defined by the sublimation temperatures of the metal precursors on the lower temperature side and the strongly accelerated desorption of precursors on the higher temperature side. All the processes show the same behavior, i.e. the film growth rate decreases with increasing deposition temperature, which is actually a common feature with carboxylic acid precursors in ALD/MLD.[32] Finally, we confirmed that all the processes exhibited the linear dependency of the film thickness on the number of deposition cycles, as expected for an ideal ALD/MLD process; Figure 2 (f) shows the data at 220 °C, i.e. at the temperature selected for the common deposition temperature for our final experiments.

From the data presented in Figure 2, it can be concluded that in general the GPC values are of the same level for all the processes, i.e. ~3 Å/cycle at 220 °C. Interestingly, the lowest GPC values are for the K- and Sr-based processes, and not for the processes with the smallest alkali and alkaline earth metals. This suggests that the GPC is controlled by at least two competing factors: the size and the reactivity of the metal cation. The smaller

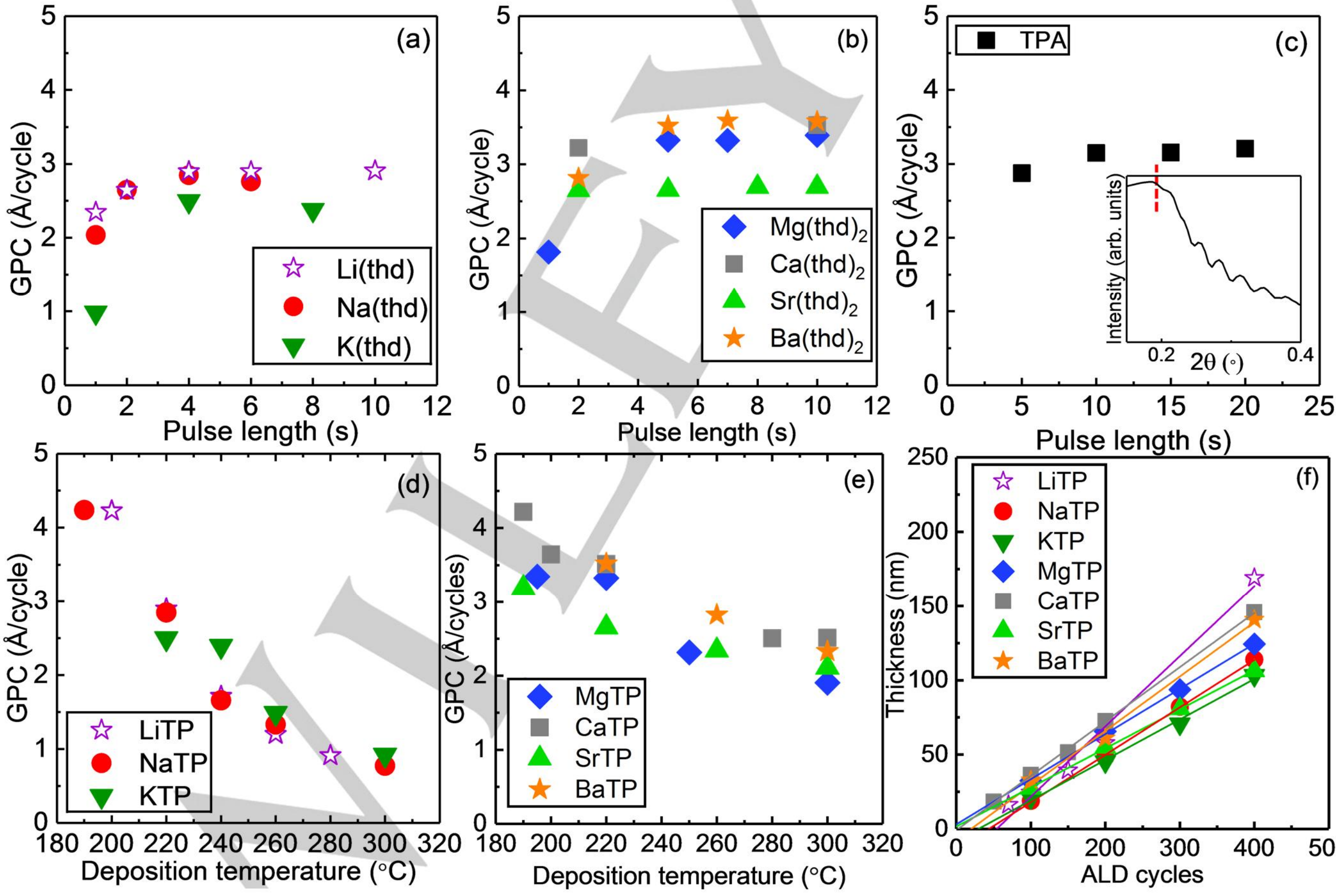

Figure 2. Growth-per-cycle (GPC) values for (a) alkali and (b) alkaline earth metal terephthalate thin films as a function of the metal precursor pulse length (TPA pulse length 10 s), (c) sodium terephthalate thin films as a function of the TPA pulse length (Na(thd) pulse length 4 s), and (d) alkali and (e) alkaline earth terephthalate thin films as a function of deposition temperature; (f) thickness of the films as a function of the number of ALD/MLD cycles. In (a) – (c) and (f), the deposition temperature was 220 °C, in (a) – (e) the number of ALD/MLD cycles was 400, and in (d) – (f) the metal/TPA precursor pulse lengths were 4-5 s/ 10-15 s. The inset in (c) displays a typical XRR curve for the metal terephthalate thin films and dashed line indicates the position of critical angle.

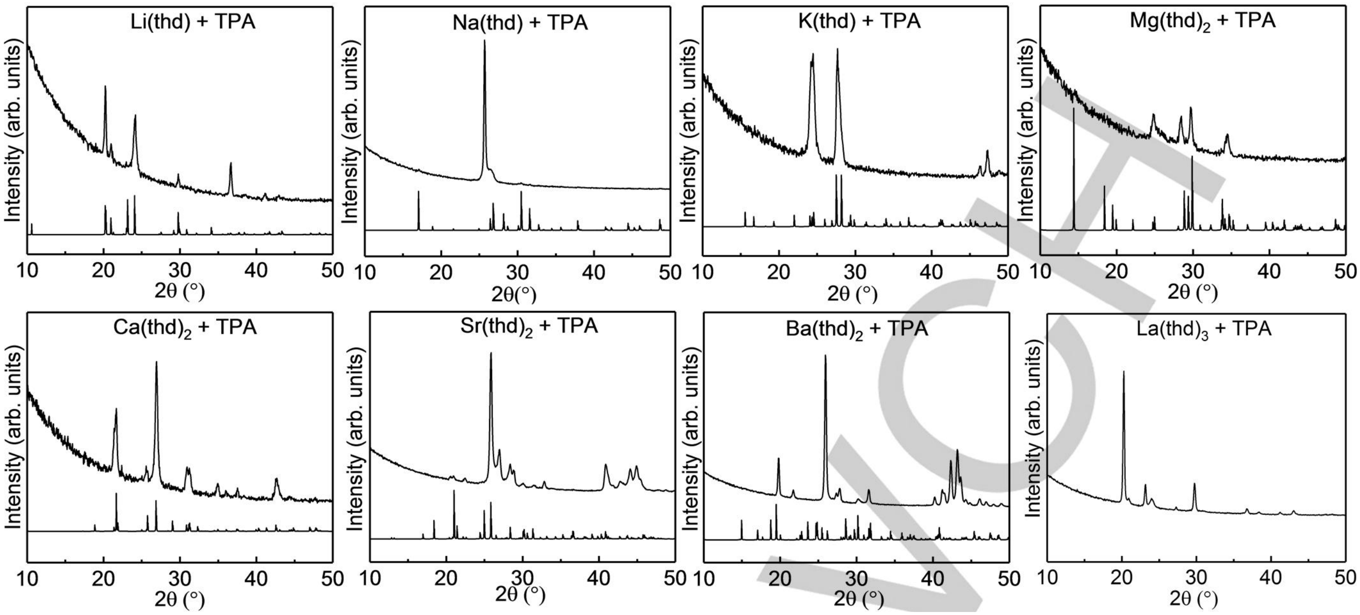

Figure 3. GIXRD patterns for thin films deposited at 220 °C through the M-thd + TPA processes. Patterns calculated from reported crystal structures[11–14,16] using Vesta software are shown below each experimental pattern. The number of ALD/MLD cycles was 400 for M = Li, K, Mg, Ca, and 1000 for M = Na, Sr, Ba, La.

Li^+, Mg^{2+} and Ca^{2+} ions are hard cations and thus more reactive. Also, for crystalline thin films the crystal structure, i.e. the way of atomic packing, is likely to affect the GPC value. This is an important fact to note, as our metal-TP films possess different crystal structures.

The GIXRD patterns collected for the as-deposited M-TP thin films are displayed in Figure 3. Most importantly, all the as-deposited films are indeed crystalline. For the discussion of the crystal structures of these new M-TP thin-film materials, we display in Figure 3 below the corresponding thin-film data, XRD patterns calculated for Li_2TP, K_2TP, CaTP, SrTP and BaTP structures (c.f. Figure 1) based on the structure data reported for powder samples in literature. Taking into account the fundamental fact that GIXRD for thin films is likely to yield peak intensities that are different from those by XRD for powder samples, we may conclude that the GIXRD patterns for our metal-TP thin films do resemble the corresponding XRD patterns to some extent; the question whether the thin film structures are exactly identical or not with the corresponding bulk structures remains to be verified with future detailed studies. For the as-deposited Mg-based film the GIXRD pattern is consistent with the water-containing $MgC_8H_4O_4(H_2O)_2$ structure reported for bulk samples and shown in Figure 1. We also carried out few depositions with the precursor combination, La(thd)$_3$ + TPA, as lanthanum resembles the largest s-block metals. Interestingly, these films are crystalline as well (Figure 3) even though there are no reports of La-TP compounds in literature.

In order to investigate the water absorption/desorption characteristics of the films, the as-deposited thin-film samples were exposed to repeated humidity (75% relative humidity) and thermal (300 °C, air) treatments; representative GIXRD data collected after the treatments are shown in Figure 4. For the Li_2TP, Na_2TP, K_2TP, BaTP and La_2TP_3 films no changes in GIXRD pattern were seen during the standard storage at ca. 30% relative humidity or upon the aforementioned treatments; these patterns are hence not shown in Figure 4. For the as-deposited water-containing $MgTP(H_2O)_2$ film the humidity treatment did not affect the crystallinity/structure whereas upon the thermal treatment the film became amorphous (Figure 4), implying that the coordinated water molecules are apparently needed to satisfy the coordination requirement of magnesium for a crystalline network. The SrTP film was found to undergo a similar reversible crystal structure change upon the humidity and heat treatments as was observed for CaTP films in our previous study.[28] The GIXRD pattern for our hydrated SrTP film (Figure 4) is essentially compatible with the peak positions calculated based on reported $SrTP(H_2O)_3$ structure.[13]

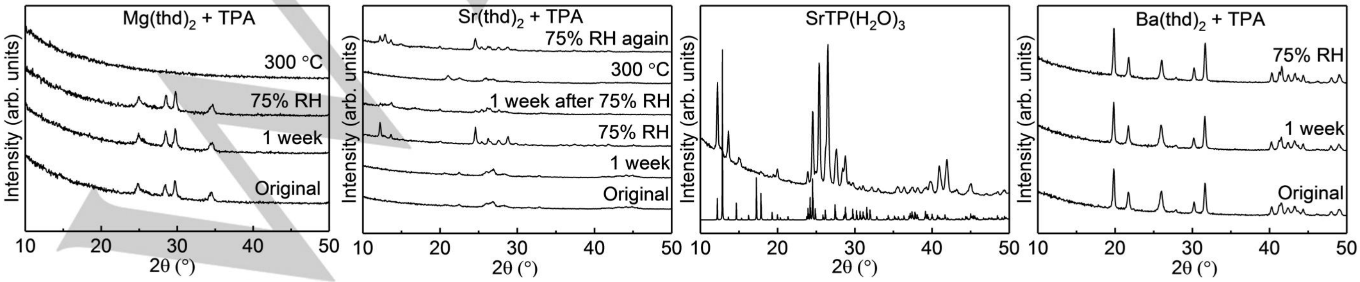

Figure 4. GIXRD patterns for selected (grown with 400 ALD/MLD cycles and thus 100-150 nm thick) as-deposited and humidity and heat treated thin films; the experimental pattern for humidity treated SrTP film is compared to the pattern calculated using Vesta software for the $SrTP(H_2O)_3$ structure.[13]

Table 1. Density values determined from XRR data for our thin-film samples in comparison to crystal structures (and ideal densities calculated from the crystal structure data) reported in literature for bulk samples.

	Li_2TP	Na_2TP	K_2TP	$MgTP(H_2O)_2$	CaTP	$CaTP(H_2O)_3$	SrTP	$SrTP(H_2O)_3$	BaTP
Ionic radius (Å)	0.76	1.02	1.38	0.72	1.00	1.00	1.18	1.18	1.35
Space group	$P2_1/c$[12]	$Pbc2_1$[12]	$P2_1/c$[12]	$C2/c$[11]	$C2/c$[8]	$P2_1/c$[8]	$P2_1/c$[13]	$P2_1/a$[13]	$Pbca$[14]
Coordination number	4	6	6	6	6	8	6	8	8
Ideal density (g/cm^3)	1.6	1.9	1.8	1.7	2.0	1.7	2.0	1.9	2.6
Present density (g/cm^3)	1.4	1.7	1.6	1.4	1.7	1.4	1.9	1.8	2.4

We employed the XRR data not only for the film-thickness determination but also to systematically investigate the densities of our different thin-film samples. As a general observation for the different materials, the density was found to first somewhat decrease with increasing film thickness and then stay constant. In Table 1, we compare these "saturated" density values to the ideal densities calculated from the crystal structure data reported for relevant bulk samples. It is seen that the density values for our thin films are systematically slightly lower than the ideal values calculated from the reported crystal structures. Also seen is that the hydrated metal terephthalates have lower densities than the corresponding anhydrous metal terephthalates; apparently the water coordination creates more empty space in the structure.[9,10]

With increasing number of ALD/MLD cycles the film surface structure apparently becomes more uniform, as was already shown using AFM in our earlier study for the Li_2TP films.[29] We also examined our CaTP films with AFM in our previous study;[28] the experiments showed that the surface roughness increases with increasing film thickness, which is rather expected for in-situ crystallized thin films. Also the grain/crystallite size increased with the film thickness. Here we investigated two BaTP thin-film samples grown with 100 and 400 ALD/MLD cycles, see Figure 5. The conclusions revealed from the AFM images for BaTP are highly parallel to those for Li_2TP and CaTP, i.e. with increasing film thickness both the grain size and the RMS surface rourghness increase. In general, the RMS roughness values are in the order of few nanometers for our films, e.g. 2.6 nm for a 36-nm thick BaTP film. The observed increase in the grain size with increasing film thickness points towards an island-type growth mode. This could also explain the observed decrease in density.

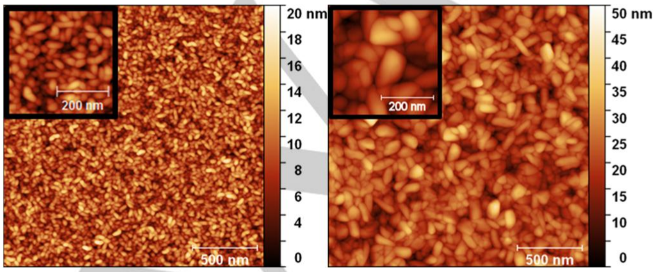

Figure 5. AFM images for BaTP films with 100 (left) and 400 (right) ALD/MLD cycles: the RMS roughness values are 2.6 nm (film thickness 36 nm) and 5.6 nm (film thickness 129 nm), respectively.

The crystal structures tentatively assigned for the anhydrous and hydrated films were further corroborated from Fourier transform infrared (FTIR) spectra, see Figure 6. First of all, in the region of 1700 cm^{-1} no peaks due to free COOH groups are seen, which confirms that during the ALD/MLD process the carboxylic acid precursor completely reacts to form the carboxylate-metal bond as expected. The dominant absorption bands seen in the spectra arise from the symmetric and asymmetric stretching of the carboxylate group, respectively.[33] For all our samples, the peak separation is within ca. 130-200 cm^{-1}, being compatible with the expected structures where the metal is in a bridging position.[22]

The FTIR data also confirm that our alkali terephthalate films do not absorb water into the structure as for these films no features are seen in the 3400 cm^{-1} region arising from OH$^-$ groups even upon elongated humidity treatments. The same applies to BaTP and La_2TP_3 films as well, while for the hydrated phases in the MgTP, CaTP and SrTP systems the 3400 cm^{-1} region reveal the expected absorption band arising from OH$^-$ groups.

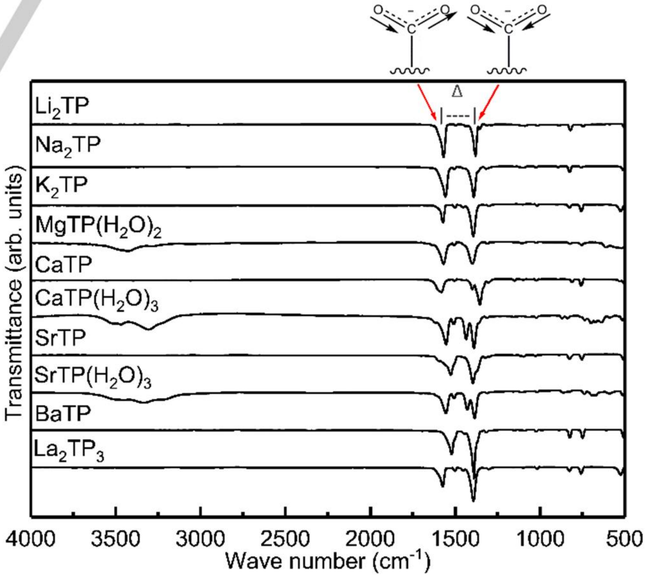

Figure 6. FTIR spectra for the anhyrous and hydrated metal-TP thin films deposited with 400 ALD/MLD cycles (ca. 100-150 nm) showing the asymmetric and symmetric stretching of the carboxylate group.

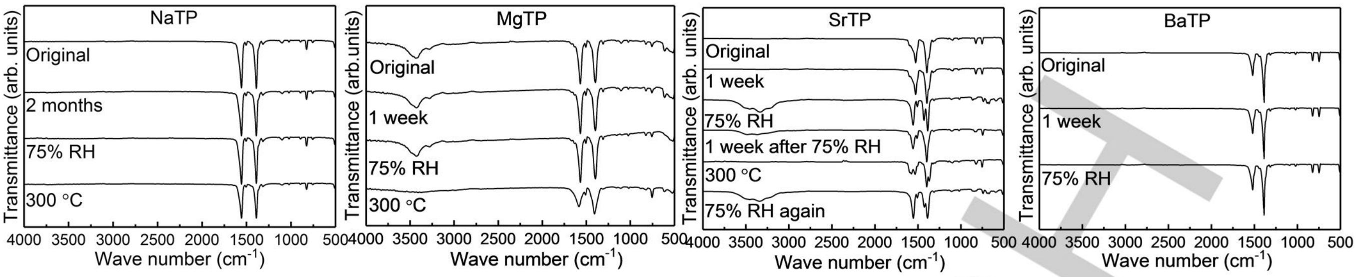

Figure 7. FTIR spectra for the Na_2TP, MgTP, SrTP and BaTP thin-film samples (400 ALD/MLD cycles and ca. 100-150 nm thick) during storage or during humidity and heat treatment experiments. Note that a behaviour similar to that shown here for Na_2TP is also seen with Li, K, Ba, and La terephthalate samples.

Finally, in Figure 7 we display representative FTIR spectra to illustrate the water absorption/desorption characteristics of MgTP and SrTP phases in comparison to Na_2TP in more detail. In particular, the fact that the as-deposited MgTP film contains water is seen as an absorption band arising from OH^- groups in the 3400 cm^{-1} region. These coordinated water molecules detach during the heat treatment at 300 °C, and as a result, the originally crystalline film becomes amorphous. The wider carboxylate absorption bands are consistent with the amorphous nature of the films with slightly varying surroundings for the COO^- group.[34] Note that crystalline thin films typically have sharp carboxylate absorption peaks. Interestingly, the SrTP film is apparently sensitive to high humidity levels only; while it remained unaffected during the long storage at ca. 30% relative humidity, it was found to absorb water in the humidity treatment at 75% relative humidity. When this water-containing SrTP film was moved back to the 30% relative humidity condition, it was found to lose the coordinated water during a one-week storage.

Conclusions

In this work we have demonstrated that crystalline inorganic-organic coordination network thin films where terephthalate anion acts as the organic linker can be fabricated in a single-step process from gaseous precursors for the entire family of s-block metals. Our newly developed ALD/MLD processes from metal-thd and terephthalic acid precursors yield these phases within a wide deposition temperature range of at least 190–300 °C in a well reproducible manner with the atomic/molecular level control for the film thickness. Moreover, an essentially similar ALD/MLD process as used for the s-block metals was found to yield crystalline lanthanum terephthalate thin films with $La(thd)_3$ as the metal precursor. This is remarkable as there are no previous reports of lanthanum terephthalate compounds for bulk samples. Our work thus underlines the strength of the ALD/MLD technique in discovering new exciting coordination network thin-film materials that may ultimately be potential material candidates for the next-generation application in, e.g., electronics, sensors, and other high-technology products.

Intercalation of water or other guest species is essentially important for several of the potential applications of the coordination-network thin films, being either a positive or a negative factor depending on the application. Understanding of the water intercalation behavior is also important from the fundamental chemistry point of view for the s-block metal based structures with relatively ionic bonds. In this work we therefore characterized our metal terephthalate thin films for their water absorption/desorption characteristics. The behaviors of the films were found to resemble those previously reported for the corresponding bulk samples. All the alkali metal (and also La) based films remained completely resistive towards the water intercalation. Among the alkaline earth films the same applied to the Ba-based films, whereas the Mg, Ca, and Sr terephthalate films were shown to reversibly absorb and desorb water. In the case of the Mg-based films the in-situ deposited films instantaneously absorbed water, and desorption of the absorbed water molecules disrupted the crystal structure such that the films became amorphous. For the Sr-based films, on the other hand, the water absorption only occurred under humidified conditions. Among the different hydrated SrTP structures known from literature for bulk samples the GIXRD pattern for our humidity-treated SrTP films pointed towards the $SrTP(H_2O)_3$ structure.

Experimental Section

In our ALD/MLD processes we employed metal-thd complexes (thd = 2,2,6,6-tetramethyl-3,5-heptanedione; synthesized in-house) as metal precursors and terephthalic acid (TPA; benzene-1,4-dicarboxylic acid; Tokyo Chemical Industry CO., Ltd.) as the organic precursor. The depositions were carried out in a commercial flow-type hot-wall ALD reactor (F-120 by ASM Microchemistry Ltd). The solid precursors were kept in open glass crucibles inside the reactor. The reactor pressure was 3~4 mbar and nitrogen (>99.999%; Schmidlin UHPN 3000 N_2 generator) was used both as the purging and carrier gas. The thin films were deposited on Si(100) substrates (3.0×3.0 cm^2) at different temperatures in the range of 190–300 °C. The sublimation temperatures were 175, 180, 220, 117, 190, 180, 200, and 175 °C for Li(thd), Na(thd), K(thd), $Mg(thd)_2$, $Ca(thd)_2$, $Sr(thd)_2$, $Ba(thd)_2$, and $La(thd)_3$, respectively, and 180-185 °C for TPA. The pulse/purge lengths for the inorganic precursor pulses were 4 s/4 s for Li(thd), Na(thd), and K(thd) and 5 s/5 s for $Mg(thd)_2$, $Ca(thd)_2$, $Sr(thd)_2$, $Ba(thd)_2$, and $La(thd)_3$. The TPA pulse/purge length was 10 s/30 s for all other processes except 10 s/15 s for the $Ca(thd)_2$ + TPA process.

The crystallinity/crystal structure was confirmed for the films using grazing incidence X-ray diffraction (GIXRD; X'Pert Pro MPD, PANalytical; Cu K_α) measurements. Thickness was determined for each thin film sample using X-ray reflectivity (XRR) and the same equipment. In the measurements, the time per step was set at 20 and 6 s in GIXRD and XRR, respectively. For the GIXRD measurements, an incidence angle of 0.5° was used.

Density of the films was deduced from the critical angle θ_c in the XRR patterns, as follows: $\rho_e = (\theta_c^2\pi)/(\lambda^2 r_e)$, where ρ_e is the mean electron density, λ is the X-ray wavelength and r_e is the classical electron radius. By assuming the elemental composition being that of pure alkali/alkaline earth metal-TP, that is, $M_2C_8H_4O_4$/ $MC_8H_4O_4$, the mass density can be estimated from $\rho_m = (\rho_e A)/(N_A Z)$, where A is the average molar mass, N_A is Avogadro constant and Z is the average atomic number.

Atomic force microscopy (AFM; Veeco Dimension 5000; Mikromasch HQ:NSC14/AlBS tips of 8 nm typical tip radius and 5 N/m force constant) images were taken in tapping mode to investigate the surface morphology of representative thin films. For each sample, scans of 2 x 2 µm^2 (512 x 512 point resolution) were mapped to compute the RMS surface roughness.

Chemical composition/bonding was studied by Fourier transform infrared (FTIR) spectroscopy. The measurements were carried out in a transmission mode with a Nicolet Magna 750 spectrometer in range of 400–4000 cm^{-1} using a resolution of 4 cm^{-1} and analyzed from 32 measured spectra. Dry air was used for purging the chamber during the measurements. A spectrum of blank Si was subtracted from the spectra to compensate for the effect of the substrate.

The water absorption/desorption characteristics of the films were investigated in humidity and heat treatments. In the humidity treatments, thin-film sample was stored in a glass box with concentrated salt solution (NaCl) that gives 75% relative humidity (RH). The relative humidity of the laboratory air is approximately 30%. In the thermal treatment tests, the sample was heat treated in a muffle furnace (Nabertherm LT 9/11) in air at 300 °C for 15 minutes.

Acknowledgements

The present work has received funding from the European Research Council under the European Union's Seventh Framework Programme (FP/2007-2013)/ERC Advanced Grant Agreement (No. 339478), and also from the Academy of Finland (Nos. 296299 and 303452). Mr. Jarkko Etula is thanked for his help in the AFM measurements.

Keywords: atomic layer deposition • molecular layer deposition • coordination network structure • inorganic-organic hybrid • thin film

[1] J. L. C. Rowsell, O. M. Yaghi, *Microporous Mesoporous Mater.* **2004**, *73*, 3–14.
[2] D. Banerjee, J. B. Parise, *Cryst. Growth Des.* **2011**, *11*, 4704–4720
[3] O. Shekhah, J. Liu, R. A. Fischer, C. Wöll, A. Gölzhauser, C. Wöll, H. K. Chae, D. Y. Siberio-Perez, J. Kim, Y. Go, et al., Chem. Soc. Rev. **2011**, *40*, 108.
[4] D. Zacher, O. Shekhah, C. Wöll, R. A. Fischer, G. Ferey, O. M. Yaghi, M. O'Keeffe, N. W. Ockwig, H. K. Chae, M. Eddaoudi, et al., *Chem. Soc. Rev.* **2009**, *38*, 1418.
[5] M. Armand, S. Grugeon, H. Vezin, S. Laruelle, P. Ribière, P. Poizot, J.-M. Tarascon, *Nat. Mater.* **2009**, *8*, 120–125.
[6] L. Zhao, J. Zhao, Y. S. Hu, H. Li, Z. Zhou, M. Armand, L. Chen, *Adv. Energy Mater.* **2012**, *2*, 962–965.
[7] J. F. M. Oudenhoven, L. Baggetto, P. H. L. Notten, *Adv. Energy Mater.* **2011**, *1*, 10–33.
[8] L. Wang, C. Mou, Y. Sun, W. Liu, Q. Deng, J. Li, *Electrochim. Acta* **2015**, *173*, 235–241.
[9] A. C. Kizzie, A. G. Wong-Foy, A. J. Matzger, *Langmuir* **2011**, *27*, 6368–6373.
[10] K. M. Fromm, *Coord. Chem. Rev.* **2008**, *252*, 856–885.
[11] J. A. Kaduk, *Acta Crystallogr. Sect. B Struct. Sci.* **2002**, *58*, 815–822.
[12] J. A. Kaduk, *Acta Crystallogr. Sect. B Struct. Sci.* **2000**, *56*, 474–485.
[13] G. Scholz, F. Emmerling, M. Dreger, E. Kemnitz, *Zeitschrift für Anorg. und Allg. Chemie* **2013**, *639*, 689–693.
[14] S. M. F. Lo, S. S. Y. Chui, I. D. Williams, IUCr, *Acta Crystallogr. Sect. C Cryst. Struct. Commun.* **1998**, *54*, 1846–1848.
[15] G. P. Panasyuk, L. A. Azarova, M. Khaddaj, G. P. Budova, I. L. Voroshilov, T. V. Grusha, A. D. Izotov, *Inorg. Mater.* **2003**, *39*, 1292–1297.
[16] M. Mazaj, G. Mali, M. Rangus, E. Žunkovič, V. Kaučič, N. Zabukovec Logar, *J. Phys. Chem. C* **2013**, *117*, 7552–7564.
[17] S. H. Dale, M. R. J. Elsegood, *Acta Crystallogr., Sect. E: Struct. Rep. Online* **2003**, *59*, m586–m587.
[18] M. D. Allendorf, A. Schwartzberg, V. Stavila, A. A. Talin, *Chemistry* **2011**, *17*, 11372–11388.
[19] I. Stassen, D. De Vos, R. Ameloot, *Chem. - A Eur. J.* **2016**, *22*, 14452–14460.
[20] L. E. Kreno, K. Leong, O. K. Farha, M. Allendorf, R. P. Van Duyne, J. T. Hupp, *Chem. Rev.* **2012**, *112*, 1105–1125.
[21] P. Sundberg, M. Karppinen, *Beilstein J. Nanotechnol.* **2014**, *5*, 1104–1136.
[22] K. B. Klepper, O. Nilsen, H. Fjellvåg, *Dalton Trans.* **2010**, *39*, 11628–11635.
[23] S. M. George, *Chem. Rev.* **2010**, *110*, 111–131.
[24] S. M. George, B. H. Lee, B. Yoon, A. I. Abdulagatov, R. A. Hall, *J. Nanosci. Nanotechnol.* **2011**, *11*, 7948–7955.
[25] H. Van Bui, F. Grillo, J. R. van Ommen, G. Ozin, J. Aizenberg, I. O. Protod'yakonov, S. He, A. T. I. Yoong, Y. Yang, Y. Zhu, et al., *Chem. Commun.* **2017**, *53*, 45–71.
[26] K. B. Lausund, O. Nilsen, *Nat. Commun.* **2016**, *7*, 13578.
[27] E. Ahvenniemi, M. Karppinen, *Chem. Commun.* **2016**, *52*, 1139–1142.
[28] E. Ahvenniemi, M. Karppinen, *Chem. Mater.* **2016**, *28*, 6260–6265.
[29] M. Nisula, M. Karppinen, *Nano Lett.* **2016**, *16*, 1276–1281.
[30] M. Nisula, J. Linnera, A. J. Karttunen, M. Karppinen, *Chem. - A Eur. J.* **2017**, *23*, 2988–2992.
[31] Z. Giedraityte, O. Lopez-Acevedo, L. A. Espinosa Leal, V. Pale, J. Sainio, T. S. Tripathi, M. Karppinen, *J. Phys. Chem. C* **2016**, *120*, 26342–26349.
[32] K. B. Klepper, O. Nilsen, T. Levy, H. Fjellvåg, *Eur. J. Inorg. Chem.* **2011**, *2011*, 5305–5312.
[33] C. A. Téllez, S. E. Hollauer, M. A. Mondragon, V. M. Castaño, *Spectrochim. Acta, Part A* **2001**, *57*, 993–1007.
[34] K. B. Klepper, O. Nilsen, S. Francis, H. Fjellvåg, *Dalt. Trans.* **2014**, *43*, 3492–3500.

Entry for the Table of Contents (Please choose one layout)

FULL PAPER

Text for Table of Contents

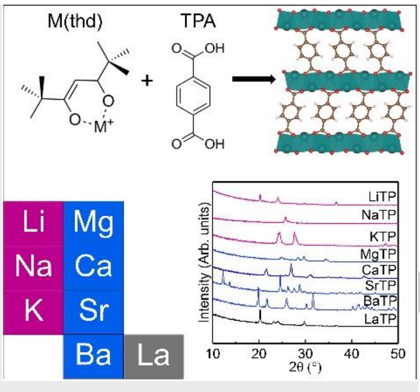

*Author(s), Corresponding Author(s)**

Page No. – Page No.

Title